"Distance mapping" and the 3–D structure of BD +30 3639

S. Akras[1][*] and W. Steffen[1,2]

[1] *Instituto de Astronomía, Universidad Nacional Autónoma de México, Ensenada, Baja California, México*
[2] *Institut für Computergraphik, Technische Universität Braunschweig, Braunschweig, Germany*

ABSTRACT

BD +30 3639 is a member of a group of uncommon planetary nebula with Wolf–Rayet central star and higher expansion velocities in [O III] than in [N II] lines. Images and high–resolution spectra from the literature are used in order to construct a 3–D model of the nebula using the morpho–kinematic code SHAPE. We find that two homologous expansion laws are needed for the [N II] and [O III] shell. We conclude that the internal velocity field of BD +30 3639 decreases with the distance from the central star at least between the [O III] and [N II] shells. A cylindrical velocity component is used to replicate the high–speed bipolar collimated outflows. We also present a new kinematic analysis technique called "distance mapping". It uses the observed proper motion vectors and the 3–D velocity field to generate maps that can be used as a constraint to the morpho–kinematic modeling with SHAPE as well as improve the accuracy for distance determination. It is applied to BD+30 3639 using 178 internal proper motion vectors from Li et al. (2002) and our 3–D velocity field to determine a distance of 1.52 ± 0.21 kpc. Finally, we find evidence for an interaction between the eastern part of nebula and the ambient H_2 molecular gas.

Key words: ISM: kinematics and dynamics – ISM: jets and outflows – methods: data analysis – planetary nebula: individual: BD +30 3639

1 INTRODUCTION

Many surveys have been made in order to discover new Planetary Nebulae (PNe) in our Galaxy (Parker & Frew 2011 and references therein) showing a variety of complex morphologies. The true 3–D dynamical structure of PNe has been a problem of great complexity for many years. According to the theoretical research, the deviation of PNe structure from the spherical symmetry occurs for several reasons (i) the presence of strong magnetic fields and/or the rotation of the central star (Garcia-Segura et al. 1997, 1999), (ii) the effect of photo–dissociation (Garcia-Segura 2010) and (iii) the binarity of central stars (Balick & Frank 2002). Morphological and kinematical studies of PNe help to understand their formation and evolution processes. High resolution spatially resolved spectroscopy offers a useful tool to interpret the structure as well as the kinematics of the nebula and to put limits to dynamical models.

The issues of determining the 3–D structure and the internal velocity field are strongly entangled. The projection on the sky flattens the structure in images and the velocity field can not be uniquely determined from Doppler-velocities and internal proper motion measurements unless restricting assumptions are made. With some basic assumptions, morpho-kinematical, radiation transfer modeling and hydrodynamical simulations (or a combination of those) can provide a reasonable estimate of the 3–D structure and velocity field.

The internal velocity along a radial ray from the central star through the nebula can show much more complex profiles ("V–" or "W–shape") than the commonly found velocity field of a single shell (Fig. 1). Such non-monotonic fields have been reported in hydrodynamic models (Perinotto et al. 2004), inferred with photoionization models (Gesicki et al. 2003, Gesicki & Zijlstra 2003) and observationally derived by Sabbadin et al. (2006). The expansion law of the separate shells are usually more closely matched by the so-called "Hubble-law" or homologous expansion. As investigated by Steffen et al. (2009), there may be significant deviations from homologous expansion even within a single shell, rendering the assumption of a homologous velocity field as insufficient for the reconstruction of the 3–D structure. In such cases, additional information or assumptions, such as some sort
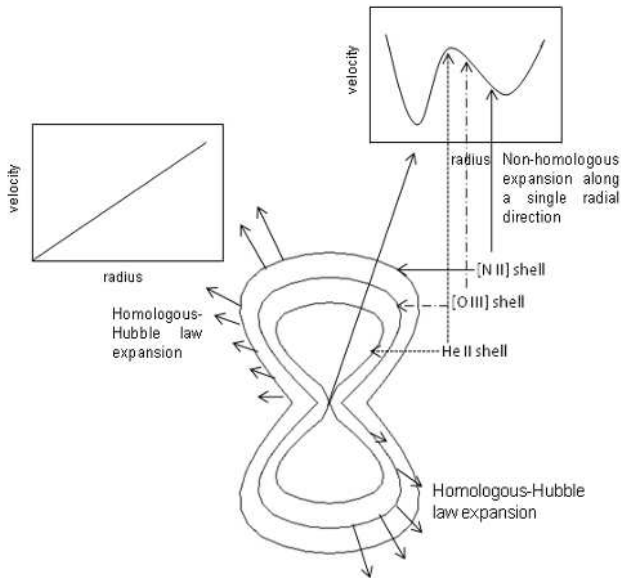
---

[*] e-mail:akras@astrosen.unam.mx

Figure 1. A sketch illustrating the internal velocity field ("V–" or "W–shape") across the whole nebula (along a single radial direction) and the homologous expansion law (Hubble–type) of a single shell (e.g. [N II] or [O III]).

of global or local symmetry properties are required for an unambiguous reconstruction.

Many PNe appear to show at least nearly a homologous expansion law based on their optical images and PV diagrams (where it is safe to assume cylindrical symmetry). High ionization ions with lower expansion velocities lay closer to the central star than low ionization ions (Wilson 1950). Nevertheless, there is a group of uncommon PNe which shows a reverse behaviour (higher expansion velocities at high ionization ions (e.g. [O III]) than low ionization ions (e.g. [N II])). This group includes BD+30 3639, NGC 40, IC 351, NGC 6369, M1-32, NGC 1501, NGC 2022 and NGC 6751 (Medina et al. 2006). Most of them also display a non-spherical structure.

Regarding the morphology of PNe, the fraction of spherically and non–spherically symmetric PNe in our Galaxy has been found at 19 per cent and 81 per cent, respectively (Parker et al. 2006; Miszalski et al. 2008). Spatially resolved spectroscopic observations have revealed that the seemingly spherically symmetric PNe can show a more complex structure along the line of sight. An example is the Ring Nebula (Bryce et al. 1994, Guerrero et al. 1997, Steffen et al. 2007) or BD +30 3639 (Bryce & Mellema 1999). Therefore finding the orientation of PNe poses a crucial problem to recognize their true 3–D structure (Balick & Frank 2002). Furthermore, the morphology of PNe is likely to be related to the presence of magnetic fields or binary central stars. In order to resolve the role of magnetic field and binarity in shaping of PNe, it is necessary to study the complete 3–D structure and velocity field in as many PNe as possible.

Knowledge of the 3–D structure and velocity field of PNe can also yield a significant improvement in accuracy of distance determination, which still poses a key problem in PNe research. The lack of a reliable general method to determine the distance of PNe still remains a great problem. Although, many attempts have been made to evaluate the distance of PNe using several methods like the trigonometric parallax, expansion parallax and statistical, their results are often discrepant (Guzmán et al. 2009).

However, in the last few years, the expansion parallax method has become the most accurate method for measuring the distance of particular PNe by using high quality data from the interferometers or Hubble Space Telescope (HST) by analyzing two epochs of images.

The accuracy of the expansion parallax method depends on (i) the non-spherically symmetric expansion of PNe (Phillips 2005a) and (ii) the difference between the angular expansion velocites on the sky and the material velocity (Mellema 2004; Schönberner, Jacob & Steffen 2005). The authors claim that the measured distance from expansion parallax method may be underestimated and has to be corrected by a factor of 1.1–1.5. Therefore, a detailed 3–D structure and velocity field are required to determine the distance with higher accuracy. With the 3–D morpho-kinematic code SHAPE (Steffen & López 2006, Steffen et al. 2011), in combination with suitable data, we are able to study simultaneously the rather complex 3–D structures and velocity fields of PNe.

The aim of this work is to obtain a comprehensive kinematic study of BD+30 3639 (hereafter BD+30) using high–quality images and high–resolution spectra from literature and to reconstruct a detailed 3–D morpho–kinematic model. In section 2, a description of BD+30 is presented while in section 3, we present the results from the morpho–kinematic modeling with SHAPE. The new kinematic analysis technique "distance mapping" is presented in section 4. Finally, in section 5, we discuss our results and we finish summing up our conclusions.

2   BD +30 3639

BD +30 is one of the most intensively observed PN in various wavelengths from radio (Kawamura & Masson 1996; Bryce et al. 1997), millimeter (Bachiller et al. 1991, 2000), infrared (Latter et al. 1995; Matsumoto et al. 2008), optical (Harrington et al. 1997, Bryce & Mellema 1999; Li et al. 2002) to X-rays (Arnaud, Borkowski & Harrington 1996; Kastner et al. 2000; Maness et al. 2003; Yu et al. 2009).

It is a young, compact and dense nebula with a bright Wolf-Rayet central star (WC9) with effective temperature T_{eff} =42 kK and luminosity $\log(L/L_{\odot}) = 4.71$ (Leunhagen, Hamann & Jeffrey 1996). The mass-loss rate and the wind velocity amount at $\dot{M}=1.3\ 10^{-5}\ M_{\odot}\ y^{-1}$ and 700 km s^{-1}, respectively, assuming a distance of 2.68 kpc (Hajian, Terzian & Bignell 1993). Its distance has been determined using several methods such as the expansion parallax method and statistical methods and the results vary between 0.67 kpc and 2.8 kpc (see Section 4).

High–quality images from HST show a rectangular ring shape with low emission at the central region. The emission is not uniform along its perimeter revealing a brighter region in NE and a much fainter in SW direction (see Fig. 2). The dust in the neutral envelope forms the faint optical halo by scattering the light from the central star (Harrington et al. 1997). Furthermore, high-dispersion spectra from the William Herschel Telescope (WHT) at the level of detection show an open–end shape in the [N II] lines and a closed shape
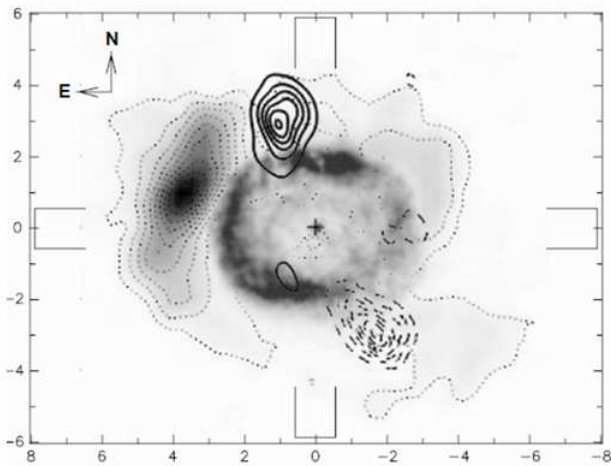
Figure 2. Several types of maps have been combined: optical (Li et al. 2002), H$_2$ (dotted contour, from Shupe et al. 1998) and CO (solid and dashed contours, from Bachiller et al. 2000).

in the [O III] lines. The [N II] shell is slightly more spatially and less spectrally extended than the [O III] shell. Bryce & Mellema (1999), based on the same data, proposed that it is a prolate nebula with low–density and fast moving polar regions, viewed almost pole–on with the inclination angle at 20 degrees. Note that NGC 40, a planetary nebula with WR–type central star as well, displays a similar structure. The dynamical ages of NGC 40 and BD+30 are 4000 years and 600–800 years, respectively, indicating the former as a more evolved version of the latter.

According to its expansion velocities, BD+30 belongs to a group of PNe which shows a non–homologous expansion. In particular, the [O III] expansion velocities are higher compared to the [N II] (35 ± 1 and 28 ± 1 km s^{-1}, respectively (Bryce & Mellema 1999); 39.5 and 21 km s^{-1}, respectively, (Medina et al. 2006)). The strong and extended X–ray emission from the hot bubble of BD+30 (T_X=3 x 10^6 K; Arnaud et a. 1996, Kastner et al. 2000), indicates a strong wind–wind interactions, and/or a high pressure bubble that drives the expansion. The intensity of X–ray emission increases from SW to NE. This direction is consistent with that of CO bullets.

A pair of strong CO (J=2-1) bullets is oriented at position angles (PA) of 20 degrees (blue–shifted) and 200 degrees (red–shifted), respectively, with projected expansion velocities of 50 km s^{-1} (Bachiller et al. 2000). The presence of the CO bullets supports the idea that the collimated outflows or strong collimated winds play a role in the evolution and formation processes of BD+30. We note that the kinematics of H$_2$ molecular gas shows an opposite expansion behavior to those of CO molecular gas, as it is expected for a prolate, almost pole–on PN. Particularly, the NE part is redshifted by up to 60 km s^{-1} and the SW part is blueshift by the same amount (Shupe et al. 1998). Figure 2 presents images taken in different wavelength regions (optical, H$_2$ and CO).

Regarding the internal velocity field across the nebula, Neiner et al. (2000) tried to fit the nebular line profiles for various elements from different stages of ionization, assuming a constant expansion velocity at 27 km s^{-1} and a turbulent component at 15 km s^{-1}. However, the broad and split

[O III] 4959 Å line profile could not be reproduced properly since the high-speed wings/shoulders are probably produced by the collimated outflows and not by the expansion of the main nebula itself. Looking more carefully at the line profiles of [Ne III], [S III], [N I] and [S I], one can discern extended and faint wings similar to [O III] line profile (see Fig. 4 in Neiner et al. 2000). Hence, a simple constant velocity is not applicable in BD+30 and additional structural and velocity components should be taken into account in order to describe the outflows. These could be the molecular bullets and their interaction with the main nebula.

Sabbadin et al. (2006) claimed that BD +30 is a rare object with a "V-shape" velocity field. They found a decreasing function up to R=1.875 arcsec, V = 110($\pm$10) $-$ 43($\pm$5)R (R takes values between 1.725 arecsec and 1.875 arcsec) for the higher ionization ions (such as O^{++}, Ar^{++}, He^{++} and S^{++}) and an increasing velocity function V = 15.0($\pm$2)R (R takes values from 1.875 arcsec to 2.10 arcsec) for the low ionization ions (such as O^o, O$^+$, S$^+$ and N$^+$) and producing a "V-shape" velocity profile.

The same "V–shape" velocity profile has already been found for 10 Galactic PNe using the emission lines of Hα, [N II] and [O III] (Gesicki et al. 2003). Moreover, Gesicki & Zijlstra (2003) claim that they found a more complex "W–shape" velocity field in three Galactic PNe by fitting 9 nebular line profiles and covering the whole nebula from high to low ionization ions. They also found that there is an anti–corellation between the density distribution and the velocity field. Responsible for that could be the stellar winds from the WR central star of BD +30 which shows strong variations on a very short period of time (e.g. BD+30; Grosdidier, Acker, Moffat 2000 & R Hydrea; Zijlstra, Bedding & Mattei 2002) suggesting strong mass–loss fluctuations and a non-uniform density distribution.

3 SHAPE MODEL

3.1 Morpho–kinematic model

In an attempt to improve previous distance determinations we construct a more detailed morpho-kinematic model of the main nebula than those used before. Earlier models consisted of an ellipsoidal shape with a homologous expansion model (Li et al, 2002). We will include secondary deviations for this shape and from the homologous expansion model. We introduce "distance mapping" as an additional constraint for the internal structure determination and to improve the distance determination itself (see Section 4).

In order to reconstruct the 3–D structure of BD +30, we use the morpho–kinematic code SHAPE (Steffen & López 2006, Steffen et al. 2011). The observations are optical images (Harrington et al. 1997), PV diagrams for [N II] and [O III] lines from Bryce & Mellema (1999) and internal proper motion measurements by Li et al. (2002). The [O III] shell reveals bright wings with expansion velocities up to 80 km s^{-1} in both directions whereas the main nebula expands with 35–40 km s^{-1}. In the PV diagrams, the [N II] shell is more extended than the [O III] shell which is consistent with the narrow-band optical images. It expands with velocities 25-30 km s^{-1}. The simultaneous reconstruction of the [N II] and [O III] PV diagrams was therefore not possible
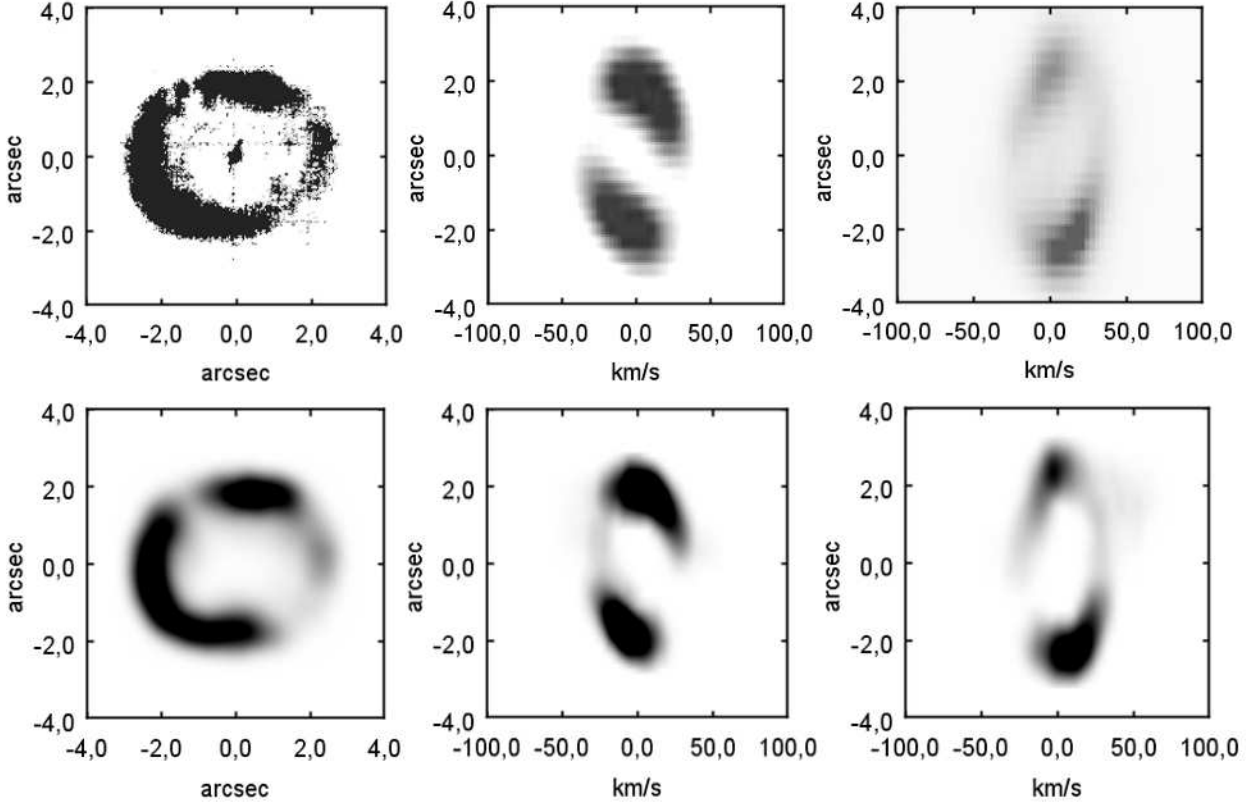
Figure 3. The observed and modeled [N II] images on the left and the corresponding synthetic PV diagrams of BD +30 3639 modeled with SHAPE. The observations are at the top (Harrington et al. 1997, Bryce & Mellema 1999) and the models at the bottom . The middle panels show the PV line profile in north–south direction and the right panels in west–east direction. The data are displayed with a square root intensity scale to show at the same time the bright main nebula and the faint high–velocity outflows. North is at the top and east at the left.

with one homologous velocity law for both, with the [O III] shell, nearly 10 per cent, closer to the central star. Thus, two velocity laws are used (V=28 r/r$_o$ km s^{-1} for the [N II] line and V=40 r/r$_o$ km s^{-1} for the [O III] line, where r is the distance from the central star and r$_o$ is the reference radius of the [N II] shell equal to 2.5 arcsec. Because the nebula is not spherically symmetric but shows a rectangular shape, the maximum distance "r" from the central star varies from 2.25 to 2.75 arcsec. Therefore, the internal velocity field of BD +30 is a decreasing function of the distance from the central star over the range of the [O III] and [N II] shell like in Figure 1.

The results of the rendered model are presented in Figures 3 & 4 (lower panels) with the observed data (upper panels). Surprisingly similar PV diagrams have been found for NGC 6369 (Steffen & López 2006) and NGC 6565 (Turatto et al. 2002). The latter shows a rectangular structure at almost the same inclination angle as BD +30 and slightly more diffuse emission at the central region (see Fig. 16 in Turatto et al. 2002).

We begin with an ellipsoidal shell model similar to that used by Li et al. (2002). Then we iteratively add detail, first to the structure and then to the velocity field. This process is done manually as described in Steffen et al. (2011). The modeled inclination and position angles are found to be

22±4 and 20±4 degrees, respectively, with the respect of the line of sight, which are consistent with the previous studies.

The upper panels of Figures 3 & 4 show the HST narrow-band images (left panels; Harrington et al. 1997) and PV diagrams (middle and right panels; Bryce & Mellema 1999) in [N II] and [O III] emission lines, respectively. The main ionized shell shows an almost rectangular shape with the major axis aligned from west to east and the minor axis along the north-south direction. The emission is not uniform around the ring as a brighter region appears in NE direction and a much fainter one in SW direction.

In the bottom panels of Figures 3 & 4 we present the modeled images (left panels) and PV diagrams (middle and right panels) in [N II] and [O III] emission lines from two different slit directions both going through the centre (NS and WE). In particular, the [N II] 6548Å and [O III] 4959 Å were obtained in NS direction (middle panels) while the [N II] 5755Å and [O III] 5007 Å in WE direction (right panels). The [N II] velocity ellipse shows almost an open-ended shape in contrast to [O III] velocity ellipse which is closed. The open-ended shape of [N II] might just be a detection problem. Figure 5 shows the mesh model of BD +30 for [N II] (upper panels) and [O III] (lower panels) showing the geometry of the system before rendering at two 2 different orientations. Panels (a) display the view as seen from the
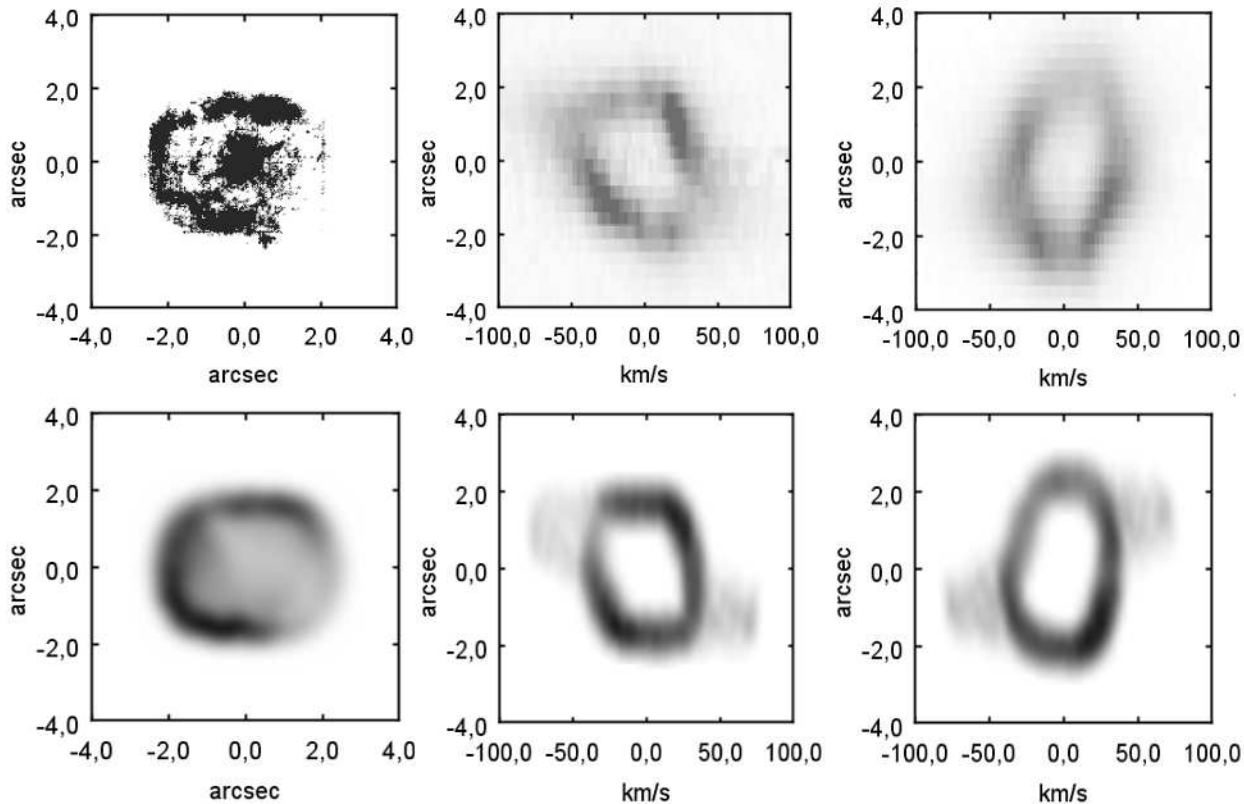
Figure 4. The observed and modeled [O III] images on the left and the corresponding synthetic PV diagrams of BD +30 3639 modeled with SHAPE. The observations are at the top (Harrington et al. 1997, Bryce & Mellema 1999) and the models at the bottom The middle panels show the PV line profile in north–south direction and the right panels in west–east direction. The data are displayed with a square root intensity scale to show at the same time the bright main nebula and the faint high–velocity outflows. North is at the top and east at the left.

observer and panels (b) display the view at 90 degrees inclination angle (edge–on).

"Criss-cross" mapping of the internal proper motion vectors shows extended and elongated structure along the direction of the molecular outflows (see Section 3.2). This is indicative for a cylindrical velocity component in the main nebula (Steffen & Koning, 2011). Even if the AGB–wind is spherically symmetric, an interaction with collimated outflows can produce an elongated elliptical PNe (Espinosa et al. 2010) and impart such a cylindrical velocity component on the main nebula. We therefore introduce a cylindrical velocity component that increases linearly away from the central star up to 30 km s^{-1} for the [N II] shell and 45 km s^{-1} for the [O III] shell. This new velocity component is added to the already existing radial one in order to reproduce the high velocity bipolar outflows along the polar direction (Fig. 4, middle panels). The cylindrical velocity component explains reasonably well the high velocity wings that Medina et al. (2006) referred and can not be reproduced by a simple homologous velocity law and a turbulent component. Finally, there is also a small random velocity component of 4.0 km s^{-1} in each Cartesian direction representing turbulent bulk motion and thermal broadening.

It is worth mentioning that the [N II] PV diagram reveals a velocity ellipse that is noticeably asymmetric in ve-

locity and brightness which is hardly seen in [O III](Fig. 3, right panels). The western bright section shows a lower expansion velocities than the eastern counterpart. We find that the model improves considerably when the velocity of the western region is reduced by 20 km s^{-1}. This asymmetry might have been caused by the interaction of the western region of the nebula with the H$_2$ molecular gas around it. The H$_2$ emission overlaps with the western part of the nebula, suggesting that it might decelerate the expansion of the nebula in this direction (see fig 1). In Fig. 6, we present the contour maps of modeled [N II] PV diagrams with the velocity of the western region being 20 km s^{-1} less (6a; blue contours) and without (6b; red contours) overlay of the observed PV diagrams (green contours).

3.2 Criss-Cross mapping

Steffen & Koning (2011) introduced "criss-cross" mapping of internal proper motion measurements and showed that it can help detect and interpret the 3–D velocity field. Applying this new technique, they also showed that the velocity field in BD+30 has deviations from a homologous velocity field. In this paper, we reapply criss-cross mapping to 178 internal proper motion vectors published by Li et al. (2002).

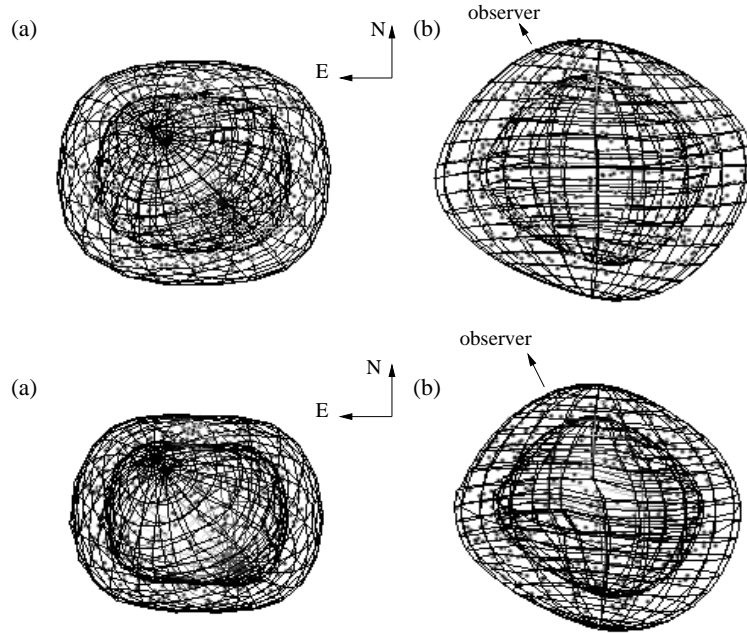The observed criss–cross map of the Hα (Fig. 7, left

Figure 5. SHAPE mesh model of BD +30 3639 for [N II] (upper panels) and [O III] (bottom panels) before rendering at two different oriantations. (a) the view as seen from the observer (north up and east to the left) and (b) the view at 90 degrees inclination angle (edge–on).
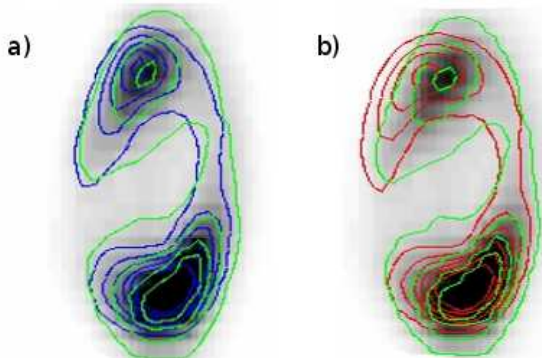

Figure 6. The observed PV diagram of [N II] with the contours of modeled PV diagram with the velocity of the western region being 20 km s^{-1} less (a) and without (b). (See the electronic version for a color version of these images.)

panel) shows clear indications that (i) the kinematic centre of the nebula is located approximately 0.5 arcsec away from the central star, even though the geometrical centre of the nebula is well centred on the star(s) and (ii) there is a cylindrical velocity component along the NE-SW direction. In contrast, the observed criss–cross map of the [N II] shows that the kinematic centre of the nebula might be located closer to the central star (Fig. 7, middle panel). The right panel in Figure 7, displays the modeled criss–cross map including a 0.25 arcsec shift of the velocity field as deduced from the observed map. Probably, the kinematic offset has been occured by a short event like a nova eruption from a binary system which has altered the homologous expansion by adding a new axisymetric component along the polar direction. RS Ophiuchi is a good example of a nova eruption

with bipolar outflows (Sokoloski et al. 2008). The scenario of a nova eruption has alredy been proposed in order to explain the high Ne abundance of BD +30 (Maness et al. 2003) and Abell 58 (Lau et al. 2011). Accordingly, in this scenario, the nova eruption could change the velocity pattern of a spherically symmetric expanding PN, at least in some regions, converting the homologous expansion to a "V–" or "W–shape" along the radial direction from the central star(s).

From the Figures 3 & 4 of Li et al. (2002), the angular deviation and the position angles (PA) from the radial direction were determined by direct measurements (Steffen & Koning, 2011). In Figure 8, we present the angular deviation as a function of PA for the Hα and [N II] lines. Both do not follow a random distribution around zero as would be expected for a radial expansion. Instead, they reveal a sinusoidal pattern which can be explained by the offset of the kinematical centre. However, the proper motion vectors of the [N II] line seem to lay closer to zero suggesting a smaller offset, consistent with the criss-cross maps. The difference between the Hα and [N II] proper motion vectors can scarcely be discerned in Figure 8. For that reason, in Figure 9, we present histograms of the observed and modeled angular deviation for PA between 155 and 335 degrees, where the difference becomes noticeable. The upper panel shows the observed Hα and [N II] histograms and the lower panel shows the modeled [N II] histograms for two offsets of the kinematic centre (0.50 arcsec; model M0.50 and 0.25 arcsec; model M0.25). The observed Hα line is consistent with the model M0.50 (black histogram), whereas the observed [N II] line is consistent with the model M0.25 (red histogram). Particularly, the former show a peak between 15 and 20 degrees whereas the latter show a peak between 5 and 10 degrees. The shift of the kinematic centre of the
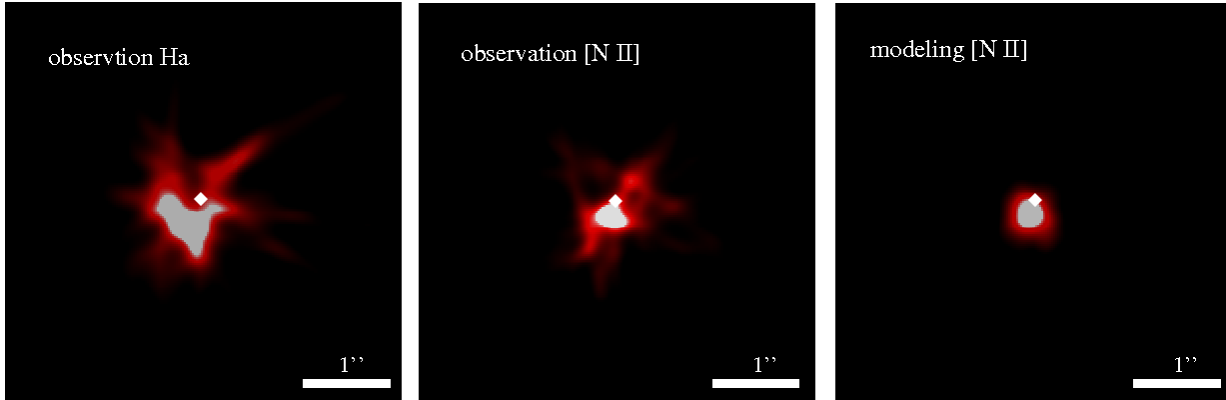
Figure 7. The observed criss-cross maps of the Hα and [N II] with the corresponding modeled criss-cross maps of the [N II]. (See the electronic version for a color version of these figures.)
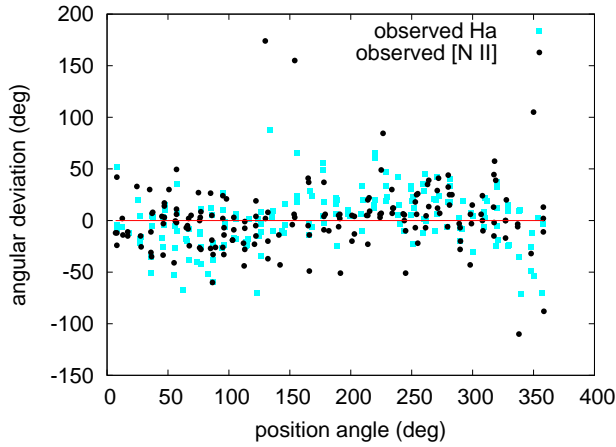

Figure 8. The angular deviation from the radial direction of the internal proper motion vectors is plotted against the position angle. The observed Hα data are in blue and the [N II] are in black (Li et al. 2002). (See the electronic version for a color version of this figure.)

nebula is confirmed for both lines. The value however, differs for Hα and [N II] probably because they represent different regions in the nebula and the effect might be different for them.

4   DISTANCE MAPPING TECHNIQUE

The distance parameter is a key problem in PNe research. Knowledge of the observed angular expansion rate and the true internal 3–D velocity field should yield a more precise and direct determination of the distance. This information can be derived from observations of internal proper motion using high quality data either from interferometers or HST and analyzing two epochs of images and Doppler-shift of the gas, combined with a 3–D morpho-kinematic model.

The basic idea is to determine the distance for small boxes throughout the 2–D image of a nebula using as many proper motion vectors as possible and generate a map of the distances obtained. In the ideal case, obviously, the distance for each box should be the same and the resulting distance
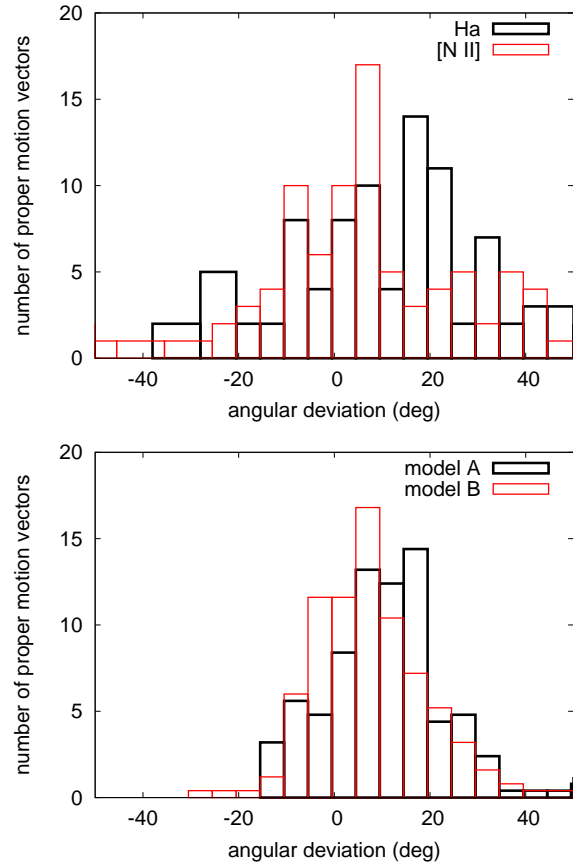

Figure 9. The angular deviation histograms of the observed Hα (black color) and [N II] (red color) data (upper panel) and of the modeled [N II] data for two offsets of the kinematic centre of the nebula, 0.50 arcsec (black color; model M0.50) and 0.25 arcsec (red color; model M0.25) (lower panel) for PA between 155 and 335. (See the electronic version for a color version of these figures.)

maps should result in a uniform value within the noise limits. Any systematic deviation hint towards deviations of the model structure and/or velocity field from the actual fields. The distance map can therefore be used as a constraint for the morpho–kinematic modeling as well as in determining distance with better accuracy.
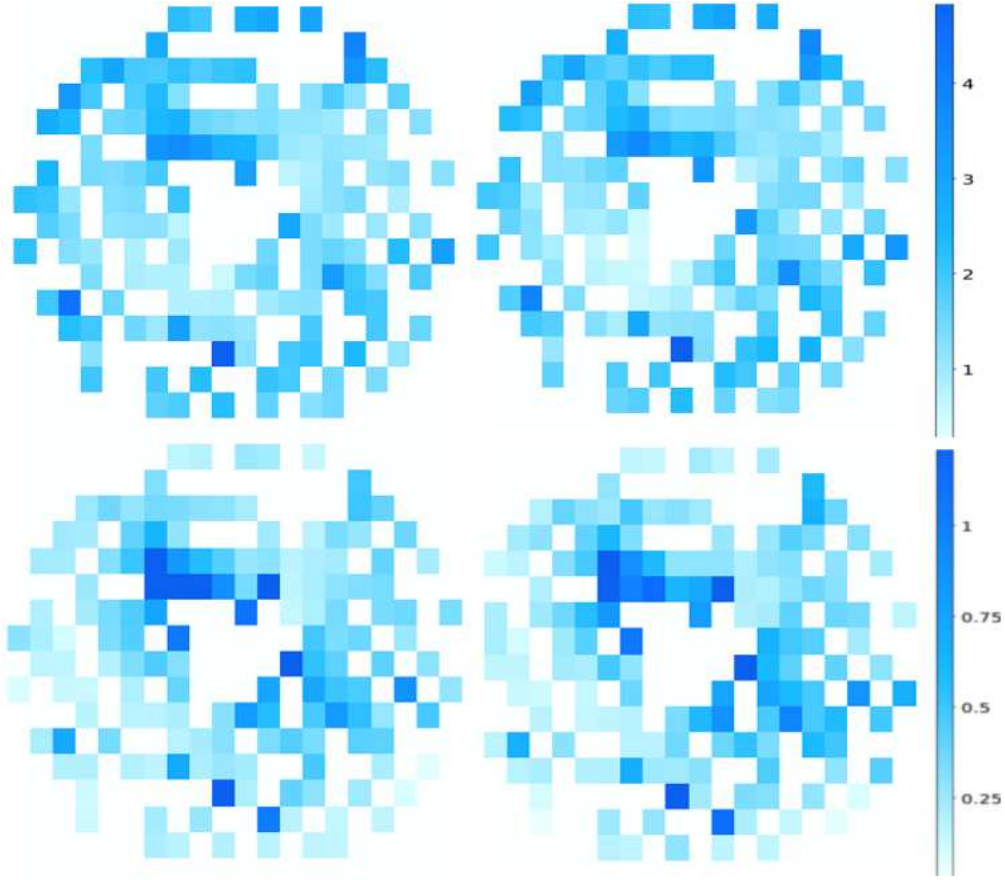
Figure 10. The distance maps (upper panels) and the error maps (lower panels) of BD +30 for two models with different offsets of the kinematic centre of the nebula (left panels: model M0.50 and right panels: model M0.25). The scale bars orrespond to the ranges indicated in units of kpc. (See the electronic version for a color version of these maps.)

In order to determine the distance of BD +30, we use our 3–D model velocity field based on the PV diagrams from Bryce & Mellema (1999) and 178 internal proper motion measurements from Li et al. (2002). We divide the nebula's image in small boxes and calculate the mean value of proper motion and tangential velocities of each one. Then, the distance and the standard deviation are calculated for each box, by means of equation (1),

$$ d = 211 \frac{V_t}{\dot{\theta}}, \qquad (1) $$

where d is the distance in kpc, V_t is the modeled tangential velocity in km s^{-1} and $\dot{\theta}$ is the observed proper motion in mas/yrs. From these data we obtain a distance for each box and then construct map of the distance and its formal error (Fig. 10). Finally, we calculate the weighted mean value to find the best distance and the corresponding statistical error σ.

Figure 10 presents the distance maps for two models with different offset of the kinematic centre of the nebula (left upper panel: model M0.50 and right upper panel: model M0.25) and the corresponding error maps for each model (lower panels).

According to the distance maps, there are two region, where the resulting distances are systematically less (region

A) and higher (region B) compared with the rest of the neb-ula (Fig. 11). In particular, the distances in the region A are determined 20–30 per cent less by the model M0.50 (mean value = 0.67 kpc) compared with the model M0.25 (mean value = 0.92 kpc). In the region B, the distances do not change significantly for different kinematic centre (< 10 per cent). Figure 12 shows the observed angular expansion ve-locities of Hα and [N II] lines as a function of position angle. One can see that, although both lines cover the same angular expansion velocities, there is a region between PA=100 and 135 degrees (region A), where the [N II] line shows systemat-ically higher angular expansion velocities than the Hα line, suggesting a possible systematic error. The overestimation of the angular expansion velocities in that region results in underestimating of the distance determination. It is there-fore, not clear whether they represent true features in the nebula, are deficiencies in the model or systematic error in the proper motion measurements. Probably, a more complex velocity field might be required with an additional velocity component along the direction of the bullets. We investigate this possibility below. Future observations might be needed to verify the complexity of the velocity field.

The resulting distances in the region B are higher than the rest of the nebula, due to the low angular velocities (see Fig. 12; $-30 < PA < 50$). We speculate that (i) the velocity field of BD +30 is even more complicated with significant
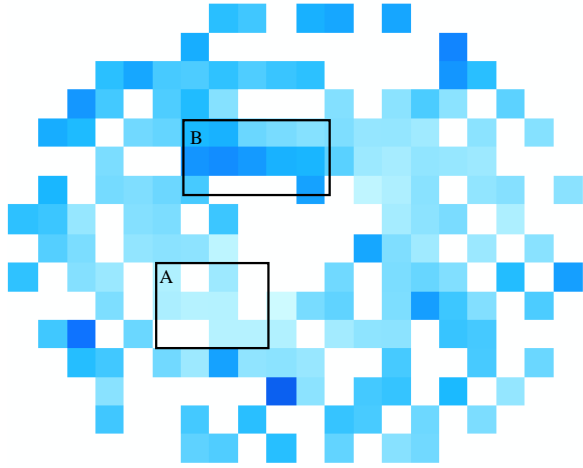
Figure 11. The distance map of the model A with the regions A and B. (See the electronic version for a color version of this map.)

Figure 12. The propor motion rate distribution is plotted against the position angle. The observed Hα data are in blue and the [N II] data are in black (Li et al. 2002). (See the electronic version for a color version of this figure.)

deviations from homologous expansion within each shell, or (ii) the current kinematic data might have systematic errors and do not help to constrain a more complex model.

The option of a more complex velocity field is investigated by introducing the effect of an additional cylindrical velocity component in a limited region around the direction of the molecular outflows. Higher cylindrical velocities give higher distances, but still within the errors. The cylindrical component does not seem to influence significantly the final distance measurement. We, finally, evaluate the distance of BD +30 at 1.58±0.21 kpc and 1.46±0.21 kpc from the model M0.50 and M0.25, respectively. However, from previous distance determinations, we point out that the distance of BD +30 is clearly less than 3.0 kpc and therefore values higher than 3.00 kpc (12 points or 8 per cent) could be excluded from our calculation. In this case, the distance is found to be 1.52±0.21 kpc and 1.40±0.20 kpc for model M0.50 and M0.25, respectively. In addition, if regions A and B are excluded from the distance determinations, we find it to be 1.55±0.21 kpc and 1.43±0.20 kpc for the models M0.50 and M0.25, respectively. All the resulting distances are within the errors and consistent with the previous studies.

Previous distance determinations of BD +30 have been performed by using several methods, such as the parallax methods in radio and optical wavelengths and statistical methods. In Table 1, we give all the measured distances of BD +30. The results from the statistical methods vary significantly by a factor of 2 or 3, whereas the recent distance measurements from the parallax method give more accurate results. Our resulting distance is determined by using almost 178 proper motion vectors and a complex 3–D velocity field improving the accuracy of the distance.

5   DISCUSSION AND CONCLUSION

Our 3–D morpho–kinematic model showed that the simultaneous reconstruction of [N II] and [O III] PV diagrams is not possible with a single homologous velocity field across the nebula. BD +30 is an uncommon PN with higher [O III]
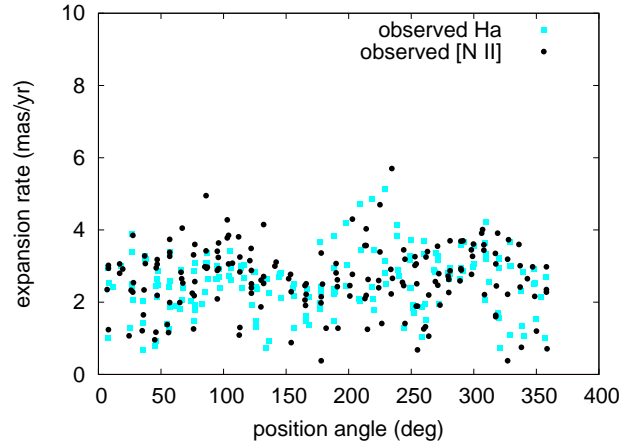
Table 1. BD +30 distances derived by different methods.

Distance (kpc)	optical/radio parallax/statis.	reference
2.80±1.37	r/p	Masson 1989
2.68±0.81	r/p	Hajian et al. 1993
1.50±0.40	r/p	Kawamura & Masson 1996
1.20±0.12	o/p	Li et al. 2002
2.57	s	Phillips 2005
0.67	s	Phillips 2002
1.85	s	Zhang 1995
2.14	s	Phillips 2004
1.16	s	Cahn et al. 1992
0.73	s	Daub 1982
1.84	s	Van de Steene & Zijlstra 1994
1.46±0.21	o/p+model	present work

expansion velocities than [N II] (Bryce & Mellema 1999; Sabbadin et al. 2006; Medina 2006).

We found that two velocity laws are necessary to model the whole structure of BD +30 (V=28 r/r$_o$ km s^{-1} for the [N II] line and V=40 r/r$_o$ km s^{-1} for the [O III] line). We concluded therefore that the internal velocity field of BD +30 is a decreasing function of the distance from the central star over the range of the [O III] and [N II] shell. This is consistent with some of the hydrodynamical models of PNe (Perinotto et al. 2004) that show complex velocity profiles with "V–"or "W–shapes". Therefore, supplementary spectroscopic observations from He I, He II, [N I], [O I] and [Ar IV] are required in order to cover the inner and the outer parts of BD +30 to obtain a more complete 3–D morpho–kinematic model.

We obtained a 3–D morpho–kinematic model that includes the main morphological and kinematical characteristics reproducing key features of the 2–D images and the position–velocity diagrams. The fast–moving collimated bipolar outflows were replicated by a cylindrical velocity component in polar direction. The inclination and position angle were found to be 22±4 and 20±4 degrees respectively, with the respect to the line of sight. We also found that

the [N II] velocity ellipse in the west–east slit direction is non–symmetric in velocity and displays low expansion at the western region, probably due to the interaction of main nebula with the ambient H_2 molecular cloud.

A new kinematic analysis technique called "distance mapping" was developed based on the 3–D velocity field and internal proper motion measurements. The distance of BD +30 was found to be 1.46±0.21 kpc in the case of a kinematic offset of 0.25 arcsec. Since, our kinematic model was built using high resolution images, PV diagrams for two slit position and 178 proper motion vectors, we expect that our resulting distance is more accurate than the previous studies. In addition, the distance mapping technique can be used to constrain morpho–kinematic models. Some problems with fitting a suitable model to the proper motion data hint towards a possible systematic error in the proper motion data. Remeasurement of the proper motion data based on the existing or new ones might be required to resolve any systematic errors. As the time baselines for high spatial resolution observations increases, detailed internal proper motion measurements can be obtained for many objects. Distance mapping can then be expected contribute significantly to the improvement of distance determination and to constrain 3–D modeling of the objects.

REFERENCES

Arnaud K., Borkowski K. J., Harrington J. P., 1996, ApJ, 462

Bachiller R., Huggins P. J., Cox P., Forveille T., 1991 A&A 247, 525

Bachiller R., Forveille T., Huggins P. J., Cox P., Maillard J. P., 2000, A&A, 353

Balick B., Frank A., 2002, ARA&A, 40, 439

Bryce M., Mellema G., 1999, MNRAS, 309, 371

Bryce M., Pedlar A., Muxlow T., Thomasson P., Mellema G., 1997, MNRAS, 284, 815

Bryce M., Balick B., Meaburn J., 1994, MNRAS, 266, 721

Cahn J. H., Kaler J. B., Stanghellini L., 1992, A&AS, 94, 399

Daub C. T., 1982, ApJ, 260, 612

Espinosa H., Frank A., Balick B., De Marco O., Kastner J. H., Sahai R., Blackman E. G., 2010, PASP, arXiv:astroph/1011.4312v1

García–Segura G., 2010, A&A, 520, 5

García–Segura G., Langer N., Różyczka M., Franco J., 1999, ApJ, 517, 767

García–Segura G., 1997, ApJ, 489, 189

Gesicki K., Acker A., Zijlstra A. A., 2003, A&A, 400, 957-969

Gesicki K., Zijlstra A. A., 2003, MNRAS, 338, 347

Grosdidier Y., Acker A., Moffat A. F. J., 2000, A&A, 364, 597

Guerrero M. A., Manchado A., Chu Y, H., 1997, ApJ, 113, 2147

Guzmám L., Loinard L., Gómez Y., Morisset C., 2009, AJ, 138, 46

Hajian A. R., Terzian Y., Begnell C., 1993, AJ, 106, 1965

Harrington J. P., Lame N. J., White S. M., Borkowski K. J., 1997, AJ, 113, 2147

Kastner J. H., Soker N, Vrtilek S, D., Dgani R., 2000, ApJ, 545, 57

Latter W. B., Kelly D. M., Hora J. L., Deutsch L. K., 1995, ApJS, 100, 159

Lau H. H. B., De Marco O., Liu X. -W., 2011, MNRAS, 410, 1870

Leuenhagen U., Hamann W. R., Jeffery C. S., 1996, A&A, 312, 167

Li J., Harrington J. P., Borkowski K., 2002, ApJ, 123, 2676–2688

Maness H. L., Vrtilek S. D., Kastner J. H., Soker N., 2003, ApJ, 589, 439.

Masson C. R., 1989, ApJ, 346, 243

Matsumoto H., Sakon I., Onaka T., Sako S., Miyata T., Kataza H., Okada Y., Okamoto Y. K., Honda M., Yamashita T., Takahashi H., Fujiyoshi T., 2008, ApJ, 677, 1120

Kawamura J., Masson C. R., 1996, ApJ, 461, 282

Medina S., Peña M., Morisset C., Stasińska G., 2006, RevMexAA, 42, 53-74

Mellema G., 2004, A&A, 416, 623

Miszalski B., Parker Q. A., Acker A., Birkby J. L., Frew D. J., Kovacevic A., 2008, MNRAS, 383, 525

Neiner C., Acker A., Gesicki K., Szczerba R., 2000, A&A, 358, 321

Parker Q. A., Frew D., 2011, in Asymmetric Planetary Nebulae V, held in Bowness-on-Windermere, U.K., 20 - 25 June 2010, eds. A. A. Zijlstra, F. Lykou, I. McDonald, and E. Lagadec, Jodrell Bank Centre for Astrophysics,

Parker Q. A., et al. 2006, MNRAS, 373, 79

Perinotto M., Schönberner D., Steffen M., Calonaci C., 2004, A&A, 414, 993

Phillips J. P., 2005, MNRAS, 362, 847

Phillips J. P., 2004, MNRAS, 353, 589

Phillips J. P., 2002, ApJS, 139,199

Sabbadin F., Turatto M., Ragazzoni R., Cappellaro E., Benetti S., 2006, A&A, 451, 937-949

Schönberner D., Jacob., Steffen M., 2005, A&A, 441, 573

Shupe D. L., Larkin J. E., Knop R. A., Armus L., Matthews K., Soifer B. T., 1998, ApJ, 498, 267

Sokoloski J. L., Rupen M. P., Mioduszewski A. J., 2008, ApJ, 685, 137

Steffen W., Koning N., Wenger S., Morisset C. & Magnor M., 2011, Transactions of Computer Graphics and Visualization, 17, 454

Steffen W., Koning N., 2011, AJ, 141, 76

Steffen W., García–Segura G., Koning N., 2009, ApJ, 691, 696

Steffen W., López J. A., Koning N., Kwok S., Riesgo H., Richer M. G., Morisset C., 2007, in Asymmetrical Planetary Nebulae IV, ed. R. L. M. Corrradi, A. Manchado & N Soker, La Palma, 2007 June 18-22

Steffen W., López J. A., 2006, RevMexAA, 42, 99

Turatto M., Cappellaro E., Ragazzoni R., Benetti S., Sabbadin F., 2002, A&A, 384, 1062-1085.

van de Steene G. C., Zijlstra A. A., 1994 A&AS, 108, 485

Yu Y.-S., Nordon R., Kastner J. H., Houck J. H., Behar E., Soker N., 2009, ApJ, 690, 440.

Wilson O., 1950, ApJ, 111, 279

Zhang C Y., 1995, ApJS, 98, 659

Zijlstra A. A., Bedding T. R., Mattei J. A., 2002, MNRAS, 334, 498